Article

Effect of Electronic Conductivities of Iridium Oxide/Doped SnO_2 Oxygen-Evolving Catalysts on the Polarization Properties in Proton Exchange Membrane Water Electrolysis

Hideaki Ohno [1], Shinji Nohara [2,3], Katsuyoshi Kakinuma [3], Makoto Uchida [3], and Hiroyuki Uchida [2,3,*]

[1] Special Doctoral Program for Green Energy Conversion Science and Technology, Integrated Graduate School of Medicine, Engineering and Agricultural Science, University of Yamanashi, 4 Takeda, Kofu 400-8510, Japan; g16dg001@yamanashi.ac.jp
[2] Clean Energy Research Center, University of Yamanashi, 4 Takeda, Kofu 400-8510, Japan; snohara@yamanashi.ac.jp
[3] Fuel Cell Nanomaterials Center, University of Yamanashi, 6-43 Miyamae, Kofu 400-0021, Japan; kkakinuma@yamanashi.ac.jp (K.K.); uchidam@yamanashi.ac.jp (M.U.)
* Correspondence: h-uchida@yamanashi.ac.jp; Tel.: +81-55-220-8619; Fax: +81-55-220-8618

Abstract: We have developed IrO_x/M-SnO_2 (M = Nb, Ta, and Sb) anode catalysts, IrO_x nanoparticles uniformly dispersed on M-SnO_2 supports with fused-aggregate structures, which make it possible to evolve oxygen efficiently, even with a reduced amount of noble metal (Ir) in proton exchange membrane water electrolysis. Polarization properties of IrO_x/M-SnO_2 catalysts for the oxygen evolution reaction (OER) were examined at 80 °C in both 0.1 M $HClO_4$ solution (half cell) and a single cell with a Nafion® membrane (thickness = 50 μm). While all catalysts exhibited similar OER activities in the half cell, the cell potential (E_{cell}) of the single cell was found to decrease with the increasing apparent conductivities ($\sigma_{app,\ catalyst}$) of these catalysts: an E_{cell} of 1.61 V (voltage efficiency of 92%) at 1 A cm^{-2} was achieved in a single cell by the use of an IrO_x/Sb-SnO_2 anode (highest $\sigma_{app,\ catalyst}$) with a low Ir-metal loading of 0.11 mg_{Ir} cm^{-2} and Pt supported on graphitized carbon black (Pt/GCB) as the cathode, with 0.35 mg_{Pt} cm^{-2}. In addition to the reduction of the ohmic loss in the anode catalyst layer, the increased electronic conductivity contributed to decreasing the OER overpotential due to the effective utilization of the IrO_x nanocatalysts on the M-SnO_2 supports, which is an essential factor in improving the performance with low noble metal loadings.

Keywords: proton exchange membrane water electrolysis; anode catalyst; oxygen evolution reaction; iridium; tin oxide

1. Introduction

Proton exchange membrane water electrolysis (PEMWE) is an attractive method to produce high purity hydrogen with high energy conversion efficiency, even at high current densities, together with easy maintenance, start-up and shut-down [1-4]. Such superlative characteristics make PEMWE suitable for leveling of the large fluctuations of renewable energy sources when used in combination with stationary fuel cells. Conventional PEMWE cells, however, are costly because large amounts of noble metals are used as the electrocatalysts, e.g., (Ir + Pt) black at the oxygen-evolving anode (≥ 2 mg_{Ir+Pt} mg cm^{-2}) and Pt black at the hydrogen-evolving cathode (≥ 2 mg_{Pt} cm^{-2}) to maintain high conversion efficiencies with long lifetimes [2,5-7].

 doi:10.20944/preprints201811.0285.v1

Iridium-based anodes have been employed so far, in spite of the high cost and limited availability of Ir, because they have exhibited relatively high activities and high stabilities for the oxygen evolution reaction (OER) [8-10]. It is essential to develop new anode catalysts that utilize Ir more effectively, working toward much higher mass activity (*MA*, current per mass of noble metal) for the OER, as well as high durability, while clarifying the reaction mechanisms [11,12]. In order to increase the *MA*, iridium or iridium oxide (IrO_x) nanoparticles have been mixed or dispersed on various supports such as metal carbides [13-15] and oxides [16-22]. Considering the stability at the high oxygen-evolving potentials, stability in strong acidic media, and the need for high electronic conductivity, doped tin oxides have been reported as promising candidates as support materials [23,24]. Indeed, thin films and bulk powders of SnO_2 doped with Sb, Nb, Ta, In, and F have exhibited electronic conductivities ≥ 0.1 S cm^{-1}, which are sufficiently high for consideration as catalyst supports [25,26]. It has been reported that the cell potentials (E_{cell}) of PEMWE single cells with IrO_x supported on SnO_2 anodes reached values ≤ 1.65 V (≥ 90% voltage efficiency) at 1 A cm^{-2} with moderate Ir-metal loadings of 0.75 to 1 mg_{Ir} cm^{-2} [17,18,27,28]. However, the polarization performances of such catalysts are still not sufficient in the catalyst layers of single cells for the further reduction of the Ir-loading down to 1/10 of those in conventional cells, i.e., target values of ≤ 0.2 mg_{Ir} cm^{-2}. One of the reasons for this is the large contact resistance between SnO_2 particles, even though the bulk electronic conductivity of the doped SnO_2 itself is high.

Recently, Kakinuma et al. synthesized several M-doped SnO_2 (M = Nb, Ta, and Sb) materials with fused-aggregate network structures as corrosion-resistant cathode catalyst supports for polymer electrolyte fuel cells [29-31]. Unique advantages of these supports are their enhanced electronic conductivity and high gas diffusion rate. Onto such M-SnO_2 supports, we succeeded in dispersing IrO_x nanoparticles as novel anode catalysts for PEMWE. It was found that an IrO_x/Ta-SnO_2 catalyst exhibited an apparent *MA* of 15 A mg_{Ir}^{-1} for the OER in 0.1 M $HClO_4$ solution at 1.5 V vs. RHE and 80 °C, which suggests the possibility of reducing the loading of Ir in an anode catalyst to a level as low as 0.1 mg_{Ir} cm^{-2} at a voltage efficiency of 90% (E_{cell} = 1.65 V) operated at 1 A cm^{-2}, i.e. the anode potential of 1.5 V, cathode potential of −0.05 V, and the ohmic loss of the PEM of 0.10 V [32].

In the present research, we examined the polarization properties of a series of IrO_x/M-SnO_2 (M = Nb, Ta, and Sb) catalysts for the OER at 80 °C in both 0.1 M $HClO_4$ solution (half cell) and a single cell with a Nafion® membrane (thickness = 50 μm). We, for the first time, found that the E_{cell} of the single cell decreased with the increasing apparent conductivities ($\sigma_{app,\ catalyst}$) of these catalysts, whereas they exhibited similar OER activities in the half cell test. The highest performance, E_{cell} of 1.61 V (voltage efficiency = 92%) at 1 A cm^{-2} was obtained in a single cell with total noble metal loading of 0.46 mg_{Ir+Pt} cm^{-2}, in which the IrO_x/Sb-SnO_2 anode catalyst (highest $\sigma_{app,\ catalyst}$) contribute greatly.

2. Results and Discussion

2.1. Physical Properties of IrO_x/M-SnO_2 Catalysts

Figure 1 shows transmission electron microscopic (TEM) images of IrO_x/M-SnO_2 catalysts with fused-aggregate network structures. IrO_x nanoparticles of 1 to 3 nm in diameter were found to be dispersed uniformly on the oxide supports. The average sizes and the standard deviations of the IrO_x nanoparticles were 2.0 ± 0.3, 2.2 ± 0.3, and 2.0 ± 0.4 nm for the IrO_x/Nb-SnO_2, IrO_x/Ta-SnO_2, and IrO_x/Sb-SnO_2 catalysts, respectively.

We also characterized these catalysts by BET surface area (Brunauer-Emmett-Teller adsorption method) of the M-SnO_2 supports (S_{SnO2}), the iridium metal loadings, the percentage of IrO_2 (Ir^{4+}) in IrO_x, and the apparent electrical conductivities of the M-SnO_2 supports ($\sigma_{app,\ support}$) and IrO_x-dispersed catalysts ($\sigma_{app,\ catalyst}$) (see Materials and Methods). These results are summarized in Table 1. While Sb-SnO_2 exhibited a somewhat larger S_{SnO2} value, similar amounts of iridium metal were loaded with similar percentages of Ir^{4+} on all three catalysts. Marked differences are seen

Preprints (www.preprints.org) | NOT PEER-REVIEWED | Posted: 12 November 2018 doi:10.20944/preprints201811.0285.v1

between $\sigma_{app,\ support}$ and $\sigma_{app,\ catalyst}$ values for each catalyst. The Sb-SnO_2 support exhibited the highest $\sigma_{app,\ support}$ among the supports examined, i.e., three orders of magnitude higher than that of Nb-SnO_2. The $\sigma_{app,\ support}$ values of all doped-SnO_2 increased by ca. two orders of magnitude by dispersing IrO_x on their surface. In particular, the $\sigma_{app,\ catalyst}$ value of the IrO_x/Sb-SnO_2 catalyst was the highest, 8.1×10^{-1} S cm^{-1}. As reported previously for Pt/Nb-SnO_2 [33] and IrO_x/M-SnO_2 (M = Nb and Ta) [32], such an increase in the conductivity for IrO_x/Sb-SnO_2 is ascribed to the shrinkage of the depletion layer of the SnO_2 support particles [33]. Thus, we successfully synthesized IrO_x/M-SnO_2 catalysts with similar microstructures but with a range of different of $\sigma_{app,\ catalyst}$ values.

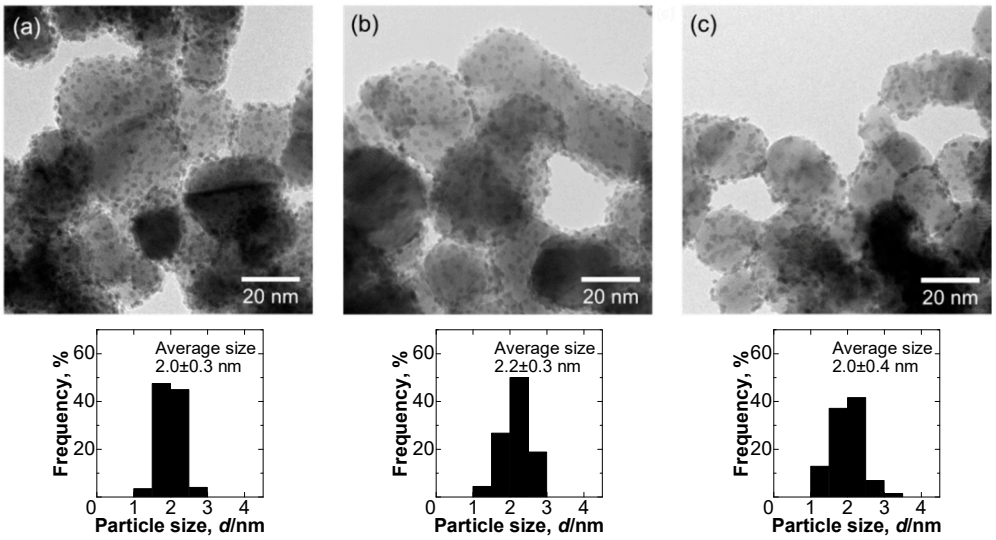

Figure 1. TEM images and particle size distribution histograms for (a) IrO_x/Nb-SnO_2, (b) IrO_x/Ta-SnO_2, and (c) IrO_x/Sb-SnO_2 catalysts. The average diameter and size distributions of the loaded IrO_x particles were estimated from ca. 300 particles in several TEM images.

Table 1. BET surface area for the supports (S_{SnO2}), Ir loadings, IrO_2 percentages (corresponding to Ir^{4+} vs. total Ir) in IrO_x nanoparticles, and apparent electrical conductivities of M-SnO_2 supports ($\sigma_{app,\ support}$) and IrO_x/M-SnO_2 catalysts ($\sigma_{app,\ catalyst}$).

Sample	S_{SnO2} ($m^2\ g^{-1}$)	Ir loading (wt%)	IrO_2 percentage	$\sigma_{app,\ support}$ (S cm^{-1})	$\sigma_{app,\ catalyst}$ (S cm^{-1})
IrO_x/Nb-SnO_2	30	11.3	16	2.5×10^{-5}	1.5×10^{-3}
IrO_x/Ta-SnO_2	25	10.4	19	1.3×10^{-4}	2.9×10^{-2}
IrO_x/Sb-SnO_2	40	11.0	21	1.8×10^{-2}	8.1×10^{-1}

2.2. Oxygen Evolution Activities of IrO_x/M-SnO_2 Catalysts in Electrolyte Solution

Figure 2a shows the *iR*-free anodic polarization curves for IrO_x/M-SnO_2 and conventional catalysts (mixture of commercial IrO_2 and Pt black, 1:1 mass ratio) in air-saturated 0.1 M $HClO_4$ solution at 80 °C, in which the current is shown as the apparent *MA*, based on the mass of Ir (or Ir + Pt for the conventional catalyst) loaded on the electrode substrate. In order to remove oxygen gas bubbles effectively from the electrode surface, the flow rate of the electrolyte solution was adjusted at 160 cm s^{-1} [32]. These IrO_x/M-SnO_2 catalysts showed onset potentials for the OER from 1.35 to 1.40 V, which was similar to that for the conventional catalyst.

Preprints (www.preprints.org) | NOT PEER-REVIEWED | Posted: 12 November 2018 doi:10.20944/preprints201811.0285.v1

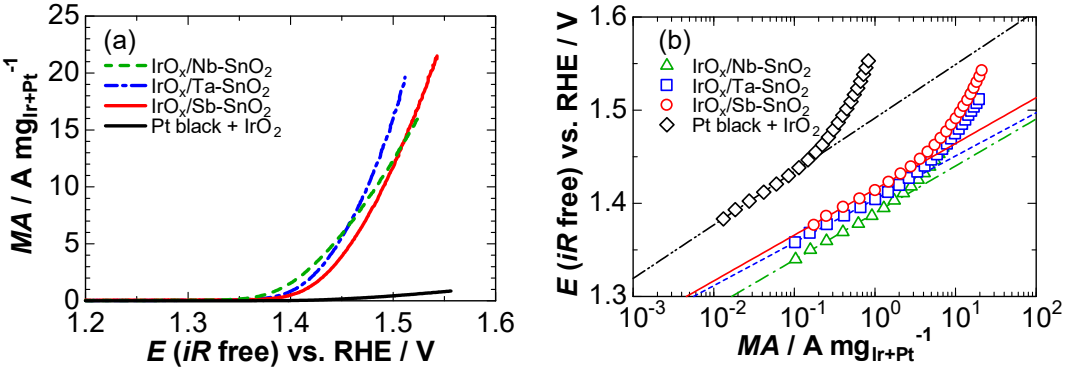

Figure 2. (a) *iR*-free anodic polarization curves for IrO_x/M-SnO_2 and conventional (IrO_2 + Pt black) catalysts in air-saturated 0.1 M $HClO_4$ solution at 80 °C with a flow rate of 160 cm s^{-1}. The current is shown as the apparent mass activity (*MA*) based on the mass of Ir (or Ir + Pt for the conventional catalyst) loaded on the electrode substrate. (b) Tafel plots for *iR*-free anodic polarization curves shown in (a). The values of Tafel slopes for IrO_x/Nb-SnO_2, IrO_x/Ta-SnO_2, IrO_x/Sb-SnO_2, and conventional catalysts at $E < 1.43$ V were 51, 46, 52, and 63 mV, respectively.

Clearly, the *MA*s of the IrO_x/M-SnO_2 catalysts were much higher than that of the conventional catalyst. The values of apparent *MA* for IrO_x/Nb-SnO_2, IrO_x/Ta-SnO_2, and IrO_x/Sb-SnO_2 at 1.5 V were 28, 36, and 27 times larger, respectively, than that of the conventional one. Such values, exceeding 10 A mg_{Ir}^{-1} on IrO_x/M-SnO_2 at 1.5 V, are with certainty due to a remarkable increase in the active surface area of the IrO_x nanoparticles, indicating the possibility of reduction of the amount of noble metal anode catalyst to a low level, e.g., 0.1 mg_{Ir} cm^{-2} for operation at 1 A cm^{-2}.

Figure 2b shows the Tafel plots for the OER at IrO_x/M-SnO_2 and conventional catalysts. Linear relationships are observed between the logarithm of *MA* and the *iR*-free potential (*E*) at $E < 1.43$ V. The Tafel slope for the conventional catalyst (63 mV) was close to the commonly reported value (60 mV) for IrO_2 electrodes in acidic solution [28,34]. In contrast, the values of Tafel slopes for IrO_x/M-SnO_2 catalysts ranged from 46 mV (IrO_x/Ta-SnO_2) to 52 mV (IrO_x/Sb-SnO_2). Such low Tafel slopes, in comparison with that of bulk IrO_x, suggests that the OER rates on the IrO_x/M-SnO_2 catalysts might be promoted by an interaction between the IrO_x nanoparticles and the doped SnO_2 supports [28,32,35]. Hence, the enhanced *MA*s of IrO_x/M-SnO_2 might be ascribed not only to a significant increase in the active surface area, by the use of IrO_x nanoparticles, but also their interaction with the oxide supports.

2.3. Oxygen Evolution Activities of IrO_x/M-SnO_2 Catalysts in a Single Cell

We prepared catalyst-coated membranes (CCMs) with low noble metal loadings by the use of the IrO_x/M-SnO_2 catalysts with 0.11 mg_{Ir} cm^{-2} at the anode and a commercial Pt/GCB (Pt supported on graphitized carbon black) with 0.35 ± 0.02 mg_{Pt} cm^{-2} at the cathode. A conventional anode catalyst (IrO_2 + Pt black, described above) with 2.66 mg_{Ir+Pt} cm^{-2} and a Pt black cathode catalyst with 2.01 mg_{Pt} cm^{-2} were employed in a reference CCM. The current-potential (*I-E*) curves of single cells operated at 80 °C are shown in Figure 3.

Preprints (www.preprints.org) | NOT PEER-REVIEWED | Posted: 12 November 2018 doi:10.20944/preprints201811.0285.v1

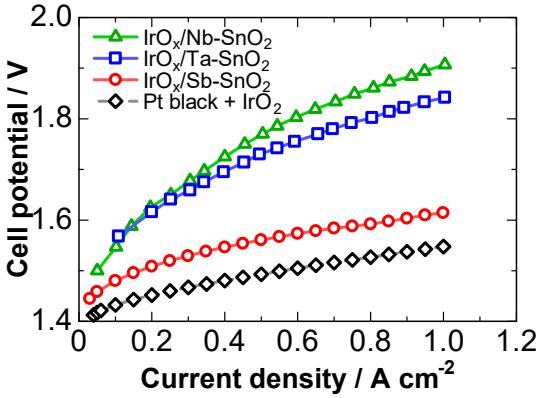

Figure 3. Steady-state *I-E* curves of single cells with various anodes and Pt/GCB cathode at 80 °C. Ultrapure water was supplied to the anode with a flow rate of 40 mL min^{-1}. The cathode compartment was purged with H_2.

The performances of the cells with three kinds of IrO_x/M-SnO_2 anodes were found to be enhanced in the order: IrO_x/Nb-SnO_2 < IrO_x/Ta-SnO_2 << IrO_x/Sb-SnO_2. For example, as shown in Table 2, the E_{cell} at 1 A cm^{-2} decreased from 1.91 V for IrO_x/Nb-SnO_2 cell to 1.61 V for the IrO_x/Sb-SnO_2 cell. The latter value was somewhat larger than that of the reference (conventional) cell (1.55 V). It is noteworthy that the initial cathode performance of Pt supported on high-surface-area carbon (Pt/C) was comparable to that of Pt black, even though Pt black has still been predominantly used in practical PEMWEs in order to ensure a long lifetime of the MEA [2]. In order to mitigate the corrosion of the carbon support, we used Pt supported on GCB in place of high-surface-area carbon. In any case, we consider that the increase in the overvoltage of our cell compared with that of the conventional cell can be ascribed predominantly to the anode catalyst with reduced amount of noble metal (< 1/20). Interestingly, the E_{cell} of 1.61 V for the IrO_x/Sb-SnO_2 cell corresponds to a voltage efficiency of 92%, which is the highest performance at the significantly low Ir loading of 0.11 mg_{Ir} cm^{-2} at the anode reported so far [28,36-38].

Table 2. Noble metal loadings on CCMs, ohmic resistances ($R_{ohm,\ cell,\ obs}$) and cell potentials (E_{cell}) at 1 A cm^{-2} for various cells.

Anode catalyst	Anode loading (mg_{Ir+Pt} cm^{-2})	Cathode loading (mg_{Pt} cm^{-2})	$R_{ohm,\ cell,\ obs}$ (mΩ cm^2)	E_{cell} @1 A cm^{-2} (V)
IrO_x/Nb-SnO_2	0.11	0.34	258	1.91
IrO_x/Ta-SnO_2	0.11	0.37	175	1.84
IrO_x/Sb-SnO_2	0.11	0.35	97	1.61
IrO_2+Pt black	2.66	2.01	75	1.55

Next, we discuss the essential parameters necessary to improve the anode performance. Referring to the properties of IrO_x/M-SnO_2 catalysts in Table 1, the only marked differences are seen for the values of $\sigma_{app,\ catalyst}$ (or $\sigma_{app,\ support}$). The ohmic resistances of the cells ($R_{ohm,\ cell,\ obs}$) measured at 1 kHz during the operation are shown in Table 2: the $R_{ohm,\ cell,\ obs}$ values ranged from 75 to 258 mΩ cm^2.

To start, we calculated values of $R_{ohm,\ cell,\ calc}$ for comparison with the observed values. First, we estimated $R_{ohm,\ anode}$ of the anode catalyst layers (CLs) as follows. The thickness of the IrO_x/Sb-SnO_2 CL was ca. 10 μm, observed by scanning ion microscopy (SIM; see Figure S2). Since we prepared all CLs in the same manner, we assumed the identical thickness for the IrO_x/Ta-SnO_2 and IrO_x/Nb-SnO_2 CLs. Assuming the porosity of the CLs to be 50%, we calculated their R_{ohm} values based on their $\sigma_{app,\ catalyst}$ values. The values of $R_{ohm,\ anode}$ thus calculated for IrO_x/Sb-SnO_2, IrO_x/Ta-SnO_2, and IrO_x/Nb-SnO_2 were 3, 68, and 1333 mΩ cm^2, respectively. Second, for the Nafion® electrolyte

Preprints (www.preprints.org) | NOT PEER-REVIEWED | Posted: 12 November 2018 doi:10.20944/preprints201811.0285.v1

membrane with the thickness of 50 μm, we adopted the $R_{ohm,\ Nafion}$ to be 50 mΩ cm². The $R_{ohm,\ cell}$ of the conventional cell in Table 2 was just 75 mΩ cm², which is assumed to include $R_{ohm,\ anode}$ (IrO_2 + Pt black) and $R_{ohm,\ cathode}$ (Pt black), together with contact resistances with the gas diffusion layers (Pt/Ti mesh and carbon paper, see Materials and Methods). This value of $R_{ohm,\ cell}$ agrees precisely with those of polymer electrolyte fuel cells (PEFCs) with Nafion® membrane of the identical thickness and Pt/C catalysts for the anode and cathode [39-41]. Thus, by adding the $R_{ohm,\ anode}$ of IrO_x/M-SnO_2 to 75 mΩ cm² stated above, we calculated the $R_{ohm,\ cell,\ calc}$ values to be 78, 143, and 1408 mΩ cm², for the cells with IrO_x/Sb-SnO_2, IrO_x/Ta-SnO_2, and IrO_x/Nb-SnO_2, respectively. The former two values are relatively consistent with those of $R_{ohm,\ cell,\ obs}$. However, a large discrepancy is seen between $R_{ohm,\ cell,\ obs}$ and $R_{ohm,\ cell,\ calc}$ for IrO_x/Nb-SnO_2. One of the possible reasons is that $\sigma_{app,\ catalyst}$ was measured in ambient air (low humidity) at room temperature, while $R_{ohm,\ cell,\ obs}$ was measured during operation with the anode in pure water at 80 °C. It has been shown that the electronic conductivities of SnO_2-based materials increase with humidity [42,43]. Water molecules adsorbed on the SnO_2 surface can act as electron donors, resulting in an increase in the carrier concentration near the surface. Such a tendency was shown to be more marked for SnO_2 samples with lower electronic conductivity [42,43]. Thus, it can be easily understood that the value of $R_{ohm,\ cell,\ obs}$ of IrO_x/Nb-SnO_2 (in pure water at 80 °C) could be much smaller than that of $R_{ohm,\ cell,\ calc}$. Taking into account such an effect of water on the electronic conductivity of the M-SnO_2, it is appropriate to employ $R_{ohm,\ cell,\ obs}$ as a measure of the apparent resistance of the anode catalyst layer, rather than $R_{ohm,\ cell,\ calc}$ based on $\sigma_{app,\ catalyst}$ (measured in air).

It is clearly seen in Figure 3 and Table 2 that E_{cell} decreased with decreasing $R_{ohm,\ cell,\ obs}$. However, this is not simply due to the reduction of the ohmic (*iR*) loss. For example, the reduction of the *iR* loss at 1 A cm^{-2} is only ca. 0.08 V by replacing the IrO_x/Ta-SnO_2 anode catalyst with IrO_x/Sb-SnO_2, but the reduction of the E_{cell} in such a case was as large as 0.23 V. On the other hand, the OER activities (*MA* values or Tafel slopes) of the three IrO_x/M-SnO_2 catalysts measured in 0.1 M $HClO_4$ solution in the previous section can be regarded as being at a similar level.

This interesting phenomenon can be reasonably explained as follows. As illustrated in Figure 4, for the measurement of the OER activities in 0.1 M $HClO_4$ electrolyte solution in the channel flow cell (half cell), we dispersed IrO_x/M-SnO_2 CLs uniformly on the Au substrate with the thickness corresponding to a ca. two-monolayer height of M-SnO_2 support particles (< 100 nm), intending that all catalyst particles can be in contact with the electrolyte solution. Therefore, it is expected that all of the IrO_x nanocatalyst particles are able to function without any influence of the small electronic (ohmic) resistances of such thin CLs. In contrast, for the measurement of single cell (MEA) performance, the thickness of the anode CL was 10 μm (100 times thicker than that in the half cell). Consequently, electrons generated at the IrO_x nanoparticles in the OER must be transported in the CL to the current collector (Pt/Ti), even though protons can be effectively supplied to the IrO_x surface through the electrolyte binder (ionomer) network. Hence, the higher the $\sigma_{app,\ catalyst}$ value (lower $R_{ohm,\ cell,\ obs}$) is, the lower the OER overvoltage will be in the single cell, due to an effective utilization of the IrO_x nanocatalyst particles on the M-SnO_2 support.

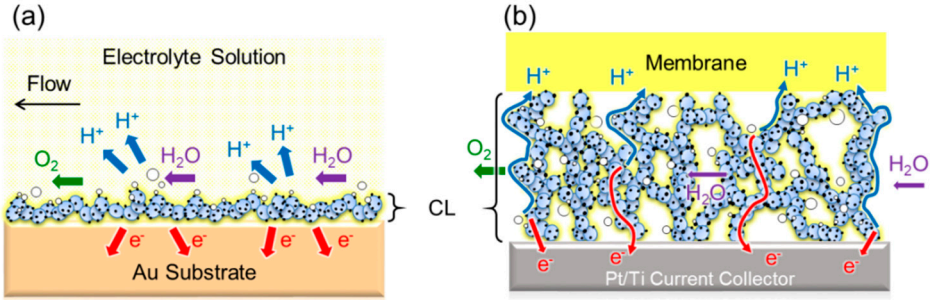

Figure 4. Schematic images of the IrO_x/M-SnO_2 anode catalyst layer (CL) during the OER in (a) electrolyte solution (half cell) and (b) a single cell.

 doi:10.20944/preprints201811.0285.v1

As is clear from Fig. 4 (b), other essential factors are the transport rates of protons and oxygen in the ionomer coated on the catalyst, in addition to the O_2 gas diffusion rate in the CL. Similar to the case of PEFC CLs [44], it is very important to control the microstructure of the CLs, i.e., thickness of the ionomer (volume ratio of ionomer to support, I/S), primary and secondary pore volumes, etc. While an effect of I/S on the performance of IrO_2/TiO_2 anode has been reported recently [45], more comprehensive research is necessary to optimize the single cell performance toward the near-ideal value evaluated in the half cell, together with high durability. Durability testing of single cells with IrO_x/Sb-SnO_2 anode catalyst is in progress in our laboratory.

3. Materials and Methods

3.1. Preparation and Characterization of IrO_x/M-SnO_2 Catalysts

The IrO_x/M-SnO_2 catalysts were prepared in the similar manner described in our previous paper [32]. Briefly, $Sn_{0.96}Nb_{0.04}O_{2-\delta}$, $Sn_{0.975}Ta_{0.025}O_{2-\delta}$, and $Sn_{0.95}Sb_{0.05}O_{2-\delta}$ (projected composition, where δ is the mole fraction of oxygen deficiencies) with the fused-aggregate network structure were synthesized by the flame pyrolysis method [29]. The surface areas of the doped SnO_2 supports were measured by the BET adsorption method (BELSORP-mini, Nippon BEL Co., Osaka, Japan). IrO_x nanoparticles were uniformly dispersed on the doped SnO_2 supports by the colloidal method. The amounts of iridium loaded on the supports were quantitatively analyzed by use of an inductively-coupled plasma mass analyzer (ICP-MS; 7500CX, Agilent Technologies Inc., Tokyo, Japan) after dissolving the IrO_x completely.

The IrO_x/M-SnO_2 catalysts were observed by TEM (H-9500, operated at 200 kV, Hitachi High-Technologies Co., Tokyo, Japan). To estimate the content of Ir^{4+}, the electronic states of iridium in the IrO_x/M-SnO_2 were characterized by X-ray photoelectron spectroscopy (XPS; JPS-9010, JEOL Co., Ltd., Tokyo, Japan) with Mg-Kα radiation (see Figure S1). The apparent electrical conductivities of the M-SnO_2 supports and IrO_x/M-SnO_2 catalysts were measured by the same method described in a previous paper [33].

3.2. Evaluation of OER Activities of Catalysts in Electrolyte Solution

The electrochemical properties of the IrO_x/M-SnO_2 catalysts were examined by a channel flow electrode cell technique [32]. The electrolyte solution used was 0.1 M $HClO_4$, which was purified in advance by conventional pre-electrolysis [46]. The working electrode consisted of Nafion®-coated supported catalyst particles uniformly dispersed on an Au substrate with a geometric area of 0.04 cm^2. The amount of the catalyst loaded was 5 μg_{Ir} cm^{-2}, which corresponds to a ca. two-monolayer height of the M-SnO_2 support particles. A mixture of commercial IrO_2 (Tokuriki Honten Co., Ltd., Tokyo, Japan) and Pt black (Ishifuku Metal Industry Co., Ltd., Tokyo, Japan) was used as a reference with 100 μg_{Ir+Pt} cm^{-2} (1:1 mass ratio). All electrode potentials are referred to the reversible hydrogen electrode, RHE.

The OER activities of the IrO_x/M-SnO_2 catalysts were evaluated by linear sweep voltammetry (LSV) at a sweep rate of 10 mV s^{-1} and 80 °C. To minimize the effect of O_2 bubbles, the 0.1 M $HClO_4$ electrolyte solution was supplied to the flow channel at a constant flow rate of 160 cm s^{-1}. To subtract *iR* loss from the polarization curve, the AC impedance of the electrolyte solution was measured by use of a frequency response analyzer (VersaSTAT 4, Princeton Applied Research, Berwyn, PA, USA) with a modulation amplitude of 10 mV in the frequency range from 10 kHz to 1 Hz.

3.3. Evaluation of Single Cell Performances

CCMs were prepared as follows. First, the anode catalyst ink was prepared by mixing the IrO_x/M-SnO_2 powder, water, ethanol, and Nafion® binder solution (DE521, Du Pont Co.) as the

 doi:10.20944/preprints201811.0285.v1

ionomer in a ball-mill for 30 min. The cathode catalyst ink was prepared from commercial Pt/GCB (Pt 50 wt%, TEC10EA50E, Tanaka Kikinzoku Kogyo, Tokyo, Japan). The I/S was adjusted to 0.7 (dry basis) in each ink. Then, the catalyst inks were directly sprayed onto the Nafion® membrane (thickness 50 μm, NRE 212, Du Pont Co., Tokyo, Japan) by the pulse-swirl-spray technique (PSS, Nordson Co., Tokyo, Japan) to prepare the CCM with an active geometric area of 25 cm^2. The CCMs were hot-pressed at 140 °C and 2.5 MPa for 3 min. The Ir loading amount for the anode CL was 0.11 mg_{Ir} cm^{-2}, and the Pt loading amount for the cathode CL was 0.35 ± 0.02 mg_{Pt} cm^{-2}. As a reference, a conventional anode catalyst (mixture of IrO_2 and Pt black, 1:1 mass ratio) with 2.66 mg_{Ir+Pt} cm^{-2} loading and a Pt black cathode catalyst with 2.01 mg_{Pt} cm^{-2} were employed. The CCM was sandwiched by two gas diffusion layers (GDLs); a Pt-plated Ti mesh (Bekaert Toko Metal Fiber Co., Ltd., Ibaraki, Japan) for the anode and a carbon fiber paper with microporous layer (25BC, SGL Carbon Group Co., Ltd., Tokyo, Japan) for the cathode. The MEA thus prepared was mounted into a single cell holder (Japan Automobile Research Institute standard cell) with ribbed single serpentine flow channels.

Ultrapure water was circulated at a flow rate of 40 mL min^{-1} for the anode. Hydrogen gas was purged to the cathode. *I-E* curves were measured galvanostatically at 80 °C under steady-state conditions. The ohmic resistance of the cell was measured by a digital AC milliohmmeter (Model 3566, Tsuruga Electric, Co.) at 1 kHz during the operation.

The thickness of the anode CL was observed after preparation of a cross-sectional sample of the CCM by SIM in a focused ion beam system (FIB, FB-2200, Hitachi High-Technologies Co., Ltd.).

4. Conclusions

The polarization performances of the IrO_x/M-SnO_2 (M= Nb, Ta, Sb) anode catalysts with fused-aggregate network structures were examined for the OER in both a half cell (0.1 M $HClO_4$) and a single cell with a Nafion® membrane at 80 °C. These catalysts exhibited similar high values of *MA* for the OER, regardless of the values of $\sigma_{app,\ catalyst}$ in the half cell, whereas the E_{cell} decreased with decreasing $R_{ohm,\ cell,\ obs,\ catalyst}$ in the single cell tests. In addition to the reduction of the *iR* loss, the predominant reduction of the anodic overvoltage is ascribed to the increased effective utilization of IrOx nanocatalyst particles supported on M-SnO_2 with higher $\sigma_{app,\ catalyst}$. Specifically, a single cell exhibited a promising performance E_{cell} = 1.61 V (voltage efficiency of 92%) at 1 A cm^{-2} and 80 °C with the use of an IrO_x/Sb-SnO_2 anode (0.11 mg_{Ir} cm^{-2}) and Pt/GCB cathode (with 0.35 mg_{Pt} cm^{-2}).

Supplementary Materials: The following are available online, Figure S1: XP spectra of IrO_x/M-SnO_2 (M = Nb, Ta, and Sb) catalysts. Figure S2: SIM image of the cross-section at the anode for the CCM with IrO_x/Sb-SnO_2 catalyst.

Author Contributions: This work was coordinated by Hiroyuki Uchida. Katsuyoshi Kakinuma prepared M-SnO_2 supports. Hideaki Ohno synthesized all IrO_x catalysts dispersed on M-SnO_2 supports and carried out all physical characterization (BET, ICP-MS, TEM, and XPS), electrochemical evaluation for the half-cell and single-cell tests. Shinji Nohara, Katsuyoshi Kakinuma, Makoto Uchida, and Hiroyuki Uchida conceived all methodologies of the experiments. All authors contributed equally to discussion for the results. Hideaki Ohno prepared the manuscript, and Hiroyuki Uchida revised the final version.

Acknowledgments: This work was supported by "Fundamental Research on Highly Efficient Polymer Electrolyte Water Electrolyzers with Low Noble Metal Electrocatalysts" from Grant-in-Aid No. 17H01229 for Scientific Research (A) from Japan Society for the Promotion of Science (JSPS). The authors appreciate Prof. Donald A. Tryk (Fuel Cell Nanomaterials Center, University of Yamanashi) for his valuable advice and Dr. Guoyu Shi (Clean Energy Research Center, University of Yamanashi) for his kind help for the single-cell tests.

Conflicts of Interest: The authors declare no conflict of interest.

References

1. Kreuter W.; Hofmann, H. Electrolysis: The Important Energy Transformer in a World of Sustainable Energy. *Int. J. Hydrogen Energy* **1998**, *23*, 661-666, 10.1016/S0360-3199(97)00109-2.
2. Carmo, M.; Fritz, D.L.; Mergel, J.; Stolten, D. A Comprehensive Review on PEM Water Electrolysis. *Int. J. Hydrogen Energy* **2013**, *38*, 4901-4934, 10.1016/j.ijhydene.2013.01.151.
3. Babic, U.; Suermann, M.; Büchi, F.N.; Gubler, L.; Schmidt T.J. Review—Identifying Critical Gaps for Polymer Electrolyte Water Electrolysis Development. *J. Electrochem. Soc.* **2017**, *164*, F387-F399, 10.1149/2.1441704jes.
4. Buttler, A.; Spliethoff, H. Current Status of Water Electrolysis for Energy Storage, Grid Balancing and Sector Coupling via Power-to-Gas and Power-to-Liquids: A Review. *Renew. Sustain Energy Rev.* **2018**, *82*, 2440-2454, 10.1016/j.rser.2017.09.003.
5. Millet, P.; Mbemba, N.; Grigoriev, S.A.; Fateev, V.N.; Aukauloo, A.; Etiévant, C. Electrochemical Performances of PEM Water Electrolysis Cells and Perspectives. *Int. J. Hydrogen Energy* **2011**, *36*, 4134-4142, 10.1016/j.ijhydene.2010.06.105.
6. Debe, M.K.; Hendricks, S.M.; Vernstrom, G.D.; Meyers, M.; Brostrom, M.; Stephens, M.; Chan, Q.; Willey, J.; Hamden, M.; Mittelsteadt, C.K.; Capuano, C.B.; Ayers, K.E.; Anderson, E.B. Initial Performance and Durability of Ultra-Low Loaded NSTF Electrodes for PEM Electrolyzers. *J. Electrochem. Soc.* **2012**, *159*, K165-K176, 10.1149/2.065206jes.
7. Aricò, A.S.; Siracusano, S.; Briguglio, N.; Baglio, V.; Blasi, A.D.; Antonucci, V. Polymer Electrolyte Membrane Water Electrolysis: Status of Technologies and Potential Applications in Combination with Renewable Power Sources. *J. Appl. Electrochem.* **2013**, *43*, 107-118, 10.1007/s10800-012-0490-5.
8. Trasatti, S. Electrocatalysis in the Anodic Evolution of Oxygen and Chlorine. *Electrochim. Acta* **1984**, *29*, 1503-1512, 10.1016/0013-4686(84)85004-5.
9. Man, I.C.; Su, H.-Y.; Calle-Vallejo, F.; Hansen, H.A.; Martinez, J.I.; Inoglu, N.G.; Kitchin, J.; Jaramillo, T.F.; Nørskov, J.K.; Rossmeisl, J. Universality in Oxygen Evolution Electrocatalysis on Oxide Surfaces. *ChemCatChem.* **2011**, *3*, 1159-1165, 10.1002/cctc.201000397.
10. Reier, T.; Oezaslan, M.; Strasser, P. Electrocatalytic Oxygen Evolution Reaction (OER) on Ru, Ir, and Pt Catalysts: A Comparative Study of Nanoparticles and Bulk Materials. *ACS Catal.* **2012**, *2*, 1765-1772, 10.1021/cs3003098.
11. Shinagawa, T.; Garcia-Esparza, A.T.; Takanabe, K. Insight on Tafel Slopes from a Microkinetic Analysis of Aqueous Electrocatalysis for Energy Conversion. *Sci. Rep.* **2015**, *5* (13801), 1-21, 10.1038/srep13801.
12. Spöri, C.; Kwan, J.T.H.; Bonakdarpour, A.; Wilkinson, D.P.; Strasser, P. The Stability Challenges of Oxygen Evolving Catalysts: Towards a Common Fundamental Understanding and Mitigation of Catalyst Degradation. *Angew. Chem. Int. Ed.* **2017**, *36*, 5994-6021, 10.1002/anie.201608601.
13. Ma, L.; Sui, S.; Zhai, Y. Preparation and Characterization of Ir/TiC Catalyst for Oxygen Evolution. *J. Power Sources* **2008**, *177*, 470-477, 10.1016/j.jpowsour.2007.11.106.
14. Nikiforov, A.V.; Tomás García, A.L.; Petrushina, I.M.; Christensen, E.; Bjerrum, N.J. Preparation and Study of IrO_2/SiC-Si Supported Anode Catalyst for High Temperature PEM Steam Electrolysers. *Int. J. Hydrogen Energy* **2011**, *36*, 5797-5805, 10.1016/j.ijhydene.2011.02.050.
15. Nikiforov, A.V.; Prag, C.B.; Polonský, J.; Petrushina, I.M.; Christensen, E.; Bjerrum, N. J. Development of Refractory Ceramics for the Oxygen Evolution Reaction (OER) Electrocatalyst Support for Water Electrolysis at Elevated Temperatures. *ECS Trans.* **2012**, *41* (42), 115-124, 10.1149/1.4718004.
16. Lee, J.-Y.; Kang, D.-K.; Lee, K.H.; Chang, D.Y. An Investigation on the Electrochemical Characteristics of Ta_2O_5-IrO_2 Anodes for the Application of Electrolysis Process. *Mater. Sci. Appl.* **2011**, *2*, 237-243, 10.4236/msa.2011.24030.
17. Xu, J.; Liu, G.; Li, J.; Wang, X. The Electrocatalytic Properties of an IrO_2/SnO_2 Catalyst Using SnO_2 as a Support and an Assisting Reagent for the Oxygen Evolution Reaction. *Electrochim. Acta* **2012**, *59*, 105-112, 10.1016/j.electacta.2011.10.044.
18. Li, G.; Yu, H.; Wang, X.; Sun, S.; Li, Y.; Shao, Z.; Yi, B. Highly Effective $Ir_xSn_{1-x}O_2$ Electrocatalysts for Oxygen Evolution Reaction in the Solid Polymer Electrolyte Water Electrolyser. *Phys. Chem. Chem. Phys.* **2013**, *15*, 2858-2866, 10.1039/c2cp44496h.
19. Hu, W.; Chen, S.; Xia, Q. IrO_2/Nb-TiO_2 Electrocatalyst for Oxygen Evolution Reaction in Acidic Medium. *Int. J. Hydrogen Energy* **2014**, *39*, 6967-6976, 10.1016/j.ijhydene.2014.02.114.

20. Kadakia, K.S.; Jampani, P.H.; Velikokhatnyi, O.I.; Datta, M.K.; Patel, P.; Chung, S.J.; Park, S.K.; Poston, J.A.; Manivannan, A.; Kumta, P.N. Study of Fluorine Doped (Nb,Ir)O_2 Solid Solution Electro-catalyst Powders for Proton Exchange Membrane Based Oxygen Evolution Reaction. *Mater. Sci. Eng. B* **2016**, *12*, 101-108, 10.1016/j.mseb.2016.06.015.
21. Oakton, E.; Lebedev, D.; Povia, M.; Abbott, D. F.; Fabbri, E.; Fedorov, A.; Nachtegaal, M.; Copéret, C.; Schmidt, T.J. IrO_2-TiO_2: A High-Surface-Area, Active, and Stable Electrocatalyst for the Oxygen Evolution Reaction. *ACS Catal.* **2017**, *7*, 2346-2352, 10.1021/acscatal.6b03246.
22. Ghadge, S.D.; Patel, P.P.; Datta, M.K.; Velikokhatnyi, O.I.; Kuruba, R.; Shanthi, P.M.; Kumta, P.N. Fluorine Substituted (Mn,Ir)O_2:F High Performance Solid Solution Oxygen Evolution Reaction Electro-catalysts for PEM Water Electrolysis. *RSC Adv.* **2017**, *7*, 17311-17324, 10.1039/c6ra27354h.
23. M. Pourbaix, *Atlas of Electrochemical Equilibria in Aqueous Solutions*, 2nd ed.; National Association of Corrosion Engineers: Houston, Texas, USA, 1974; pp. 478, 0915567989.
24. Geiger, S.; Kasian, O.; Mingers, A.M.; Mayrhofer, K.J.J.; Cherevko, S. Stability Limits of Tin-Based Electrocatalyst Supports. *Sci. Rep.* **2017**, *7* (4595), 1-7, 10.1038/s41598-017-04079-9.
25. Wang, Y.; Brezesinski, T.; Antonietti, M.; Smarsly, B. Ordered Mesoporous Sb-, Nb-, and Ta- Doped SnO_2 Thin Films with Adjustable Doping Levels and High Electrical Conductivity. *ACS Nano* **2009**, *3*, 1373-1378, 10.1021/nn900108x.
26. Oh, H.-S.; Nong, H.N.; Strasser, P. Preparation of Mesoporous Sb-, F-, and In-Doped SnO_2 Bulk Powder with High Surface Area for Use as Catalyst Supports in Electrolytic Cells. *Adv. Funct. Mater.* **2015**, *25*, 1074-1081, 10.1002/adfm.201401919.
27. Oh, H.-S.; Nong, H.N.; Reier, T.; Gliech, M.; Strasser, P. Oxide-Supported Ir Nanodendrites with High Activity and Durability for the Oxygen Evolution Reaction in Acid PEM Water Electrolyzers. *Chem. Sci.* **2015**, *6*, 3321-3328, 10.1039/c5sc00518c.
28. Liu, G.; Xu, J.; Wang, Y.; Wang, X. An Oxygen Evolution Catalyst on an Antimony Doped Tin Oxide Nanowire Structured Support for Proton Exchange Membrane Liquid Water Electrolysis. *J. Mater. Chem. A* **2015**, *3*, 20791-20800, 10.1039/c5ta02942b.
29. Kakinuma, K.; Uchida, M.; Kamino, T.; Uchida, H.; Watanabe, M. Synthesis and Electrochemical Characterization of Pt Catalyst Supported on $Sn_{0.96}Sb_{0.04}O_{2-\delta}$ with a Network Structure. *Electrochim. Acta* **2011**, *56*, 2881-2887, 10.1016/j.electacta.2010.12.077.
30. Kakinuma, K.; Chino, Y.; Senoo, Y.; Uchida, M.; Kamino, T.; Uchida, H.; Deki, S.; Watanabe, M. Characterization of Pt Catalysts on Nb-Doped and Sb-Doped $SnO_{2-\delta}$ Support Materials with Aggregated Structure by Rotating Disk Electrode and Fuel Cell Measurements. *Electrochim. Acta* **2013**, *110*, 316-324, 10.1016/j.electacta.2013.06.127.
31. Senoo, Y.; Taniguchi, K.; Kakinuma, K.; Uchida, M.; Uchida, H.; Deki, S.; Watanabe, M. Cathodic Performance and High Potential Durability of Ta-$SnO_{2-\delta}$-supported Pt Catalysts for PEFC Cathodes. *Electrochem. Commun.* **2015**, *51*, 37–40, 10.1016/j.elecom.2014.12.005.
32. Ohno, H.; Nohara, S.; Kakinuma, K.; Uchida, M.; Miyake, A.; Deki, S.; Uchida, H. Remarkable Mass Activities for the Oxygen Evolution Reaction at Iridium Oxide Nanocatalysts Dispersed on Tin Oxides for Polymer Electrolyte Membrane Water Electrolysis. *J. Electrochem. Soc.* **2017**, *164*, F944-F947, 10.1149/2.1101709jes.
33. Senoo, Y.; Kakinuma, K.; Uchida, M.; Uchida, H.; Deki, S.; Watanabe, M. Improvements in Electrical and Electrochemical Properties of Nb-Doped $SnO_{2-\delta}$ Supports for Fuel Cell Cathodes due to Aggregation and Pt Loading. *RSC Adv.* **2014**, *4*, 32180-32188, 10.1039/c4ra03988b.
34. Hu, J.-M.; Zhang, J.-Q.; Cao, C.-N. Oxygen Evolution Reaction on IrO_2-Based DSA® Type Electrodes: Kinetics Analysis of Tafel Lines and EIS. *J. Hydrogen Energy* **2004**, *29*, 791-797, 10.1016/j.ijhydene.2003.09.007.
35. Ferro, S.; Rosestolato, D.; Martínez-Huitle, C.A.; Battisti, A.D. On the Oxygen Evolution Reaction at IrO_2-SnO_2 Mixed-Oxide Electrodes. *Electrochim. Acta* **2014**, *146*, 257-261, 10.1016/j.electacta.2014.08.110.
36. Su, H.; Linkov, V.; Bladergroen, B.J. Membrane Electrode Assemblies with Low Noble Metal Loadings for Hydrogen Production from Solid Polymer Electrolyte Water Electrolysis. *Int. J. Hydrogen Energy* **2013**, *38*, 9601-9608, 10.1016/j.ijhydene.2013.05.099.
37. Lewinski, K.A.; Vliet, D.F.; Luopa, S.M. NSTF Advances for PEM Electrolysis – The Effect of Alloying on Activity of NSTF Electrolyzer Catalysts and Performance of NSTF Based PEM Electrolyzers. *ECS Trans.* **2015**, *69* (17), 893-917, 10.1149/06917.0893ecst.

38. Alia, S.M.; Rasimick, B., Ngo, C.; Neyerlin, K.C.; Kocha, S.S.; Pylypenko, S.; Xu, H.; Pivovar, B.S. Activity and Durability of Iridium Nanoparticles in the Oxygen Evolution Reaction. *J. Electrochem. Soc.* **2016**, *163*, F3105-F3112, 10.1149/2.0151611jes.
39. Omata, T.; Uchida, M.; Uchida, H.; Watanabe, M.; Miyatake, K. Effect of Platinum Loading on Fuel Cell Cathode Performance Using Hydrocarbon Ionomers as Binders. *Phys. Chem. Chem. Phys.* **2012**, *14*, 16713-16718, 10.1039/c2cp42997g.
40. Park, Y.-C.; Kakinuma, K.; Uchida, M.; Tryk, D.A.; Kamino, T.; Uchida, H.; Watanabe, M. Investigation of the Corrosion of Carbon Supports in Polymer Electrolyte Fuel Cells Using Simulated Start-Up/Shutdown Cycling. *Electrochim. Acta* **2013**, *91*, 195-207, 10.1016/j.electacta.2012.12.082.
41. Yamashita, Y.; Itami, S.; Takano, J.; Kodama, M.; Kakinuma, K.; Hara, M.; Watanabe, M.; Uchida, M. Durability of Pt Catalysts Supported on Graphitized Carbon-Black during Gas-Exchange Start-Up Operation Similar to That Used for Fuel Cell Vehicles. *J. Electrochem. Soc.* **2016**, *163*, F644-F650, 10.1149/2.0771607jes.
42. Korotchenkov, G.; Brynzari, V.; Dmitriev, S. Electrical Behavior of SnO_2 Thin Films in Humid Atmosphere. *Sens. Actuators B* **1999**, *54*, 197-201, 10.1016/S0925-4005(99)00016-7.
43. Barsan, N.; Weimar, U. Conduction Model of Metal Oxide Gas Sensors. *J. Electroceramics* **2001**, *7*, 143-167, 10.1023/A:1014405811371.
44. Lee, M.; Uchida, M.; Yano, H.; Tryk, D.A.; Uchida, H.; Watanabe, M. New Evaluation Method for the Effectiveness of Platinum/Carbon Electrocatalysts under Operating Conditions. *Electrochim. Acta* **2010**, *55*, 8504-8512, 10.1016/j.electacta.2010.07.071.
45. Bernt M.; Gasteiger, H.A. Influence of Ionomer Content in IrO_2/TiO_2 Electrodes on PEM Water Electrolyzer Performance. *J. Electrochem. Soc.* **2016**, *163*, F3179-F3189, 10.1149/2.0231611jes.
46. Uchida, H.; Ikeda, N.; Watanabe, M. Electrochemical Quartz Crystal Microbalance Study of Copper Adatoms on Gold Electrodes. *J. Electroanal. Chem.* **1997**, *424*, 5–12. 10.1016/S0022-0728(96)04924-8.